Proceedings World Geothermal Congress 2023
Beijing, China, April 17 – 21, 2023

Hot Dry Rock Preconditioning by Multi-stage Fracturing in Excavation-based Enhanced Geothermal System

Xiaotian Wu, Yingchun Li, Chun'an Tang

Deep Underground Engineering Research Center, Dalian University of Technology

wuxiaotian7099@163.com

Keywords: Excavation-based enhanced geothermal system; rock caveability; multi-stage fracturing; in-situ stress redistribution.

ABSTRACT

Rock caveability is a key factor for caving hot dry rock to stimulate reservoirs in excavation-based enhanced geothermal system (E-EGS). However, how to induce controllable hydraulic fractures to enhance rock caveability has been not fully understood. Thus, we proposed a rock preconditioning method, called multi-stage fracturing, including first-stage fracturing and second-stage fracturing. In the first-stage fracturing, fractures propagate simultaneously to optimize the in-situ stress state; then, second-stage fracturing is used to create the desired fractures based on this optimized in-situ stress state. We found that after first-stage fracturing, the minimum in-situ stress rotated nearly 90º in the region between fractures. During the second-stage fracturing, hydraulic fractures tend to propagate perpendicular to the new minimum in-situ stress and intersect with pre-existing natural fractures. These findings benefit fracture trajectory optimization and rock caveability enhancement for constructing E-EGS reservoirs.

1. INTRODUCTION

The excavation-based enhanced geothermal system (E-EGS) was proposed based on the successful mining experience in order to efficiently extract deep geothermal energy from hot dry rock (HDR) (Zhao et al. 2020). Unlike traditional enhanced geothermal systems, E-EGS stimulates geothermal reservoirs by caving rock rather than creating fracture networks, and its specific concepts and advantages were detailed in previous studies (Kang et al. 2020, Li et al. 2022). Since hot dry rock is dense and stored in the formations with high temperature and pressure, problems such as failure to start caving, caving pauses and excessive fragmentation sizes often occur over rock caving (Haraden 1992, Wang et al. 2016).

Appropriate preconditioning methods are necessary to increase the rock caveability to solve the above problems (Rafiee et al. 2015, Rafiee et al. 2016). Hydraulic fracturing can effectively precondition rock by opening existing natural fractures or inducing new hydraulic fractures (Wang et al. 2021). Studies found that when the induced hydraulic fractures intersect with the existing natural fractures, the entire HDR is unraveled into blocks, which is beneficial to reduce the fragmentation size and caving difficulty (Joubert 2010, He et al. 2016). However, a crucial problem is how to design the construction method to create desired hydraulic fractures. In-situ stress state is the main factor controlling fracture trajectories, and theoretically fractures always propagate perpendicular to the minimum in-situ stress, which means that in reverse fault formations (e.g., Yangbajing project and Ogachi project), both hydraulic and natural fractures are horizontal or sub-horizontal and parallel to each other (Pollack et al. 2020, Li et al. 2022,). Therefore, optimizing in-situ stress state is an effective measure to control the fracture propagation trajectory and improve the preconditioning effect.

To optimize in-situ stress state and obtain desired fractures, we proposed a multi-stage fracturing method, including first-stage fracturing and second-stage fracturing. In the first-stage fracturing, the simultaneous propagation of multiple fractures creates stress shadowing and changes the in-situ stress state. Then, the second-stage fracturing is performed based on the changed in-situ stress state to induce desired fractures and enhance rock caveability.

2. MODEL DESCRIPTION

In reverse fault formations, the minimum in-situ stress is vertical (Li et al. 2022). During the first-stage fracturing, the perforation clusters are set perpendicular to the minimum in-situ stress, and hydraulic fractures expand horizontally (Fig. 1a). It is found that the minimum in-situ stress is rotated by nearly 90º in the region between fractures, which will be detailed in Section 3.1. Based on the optimized in-situ stress state, horizontal wells are drilled in the region between fractures, which favors the induction of desired hydraulic fractures. However, previous rock caving experience has shown that drilling horizontal wells in formations with several hundred meters thick is highly difficult and uneconomical (Liu et al. 2022). Therefore, the inclined well is drilled, and the angle between the perforation clusters and the minimum in-situ stress is 45º (Fig. 1b). The numerical models are established based on the extended finite element method in ABAQUS software, and its physical and mechanical properties are shown in Table 1.

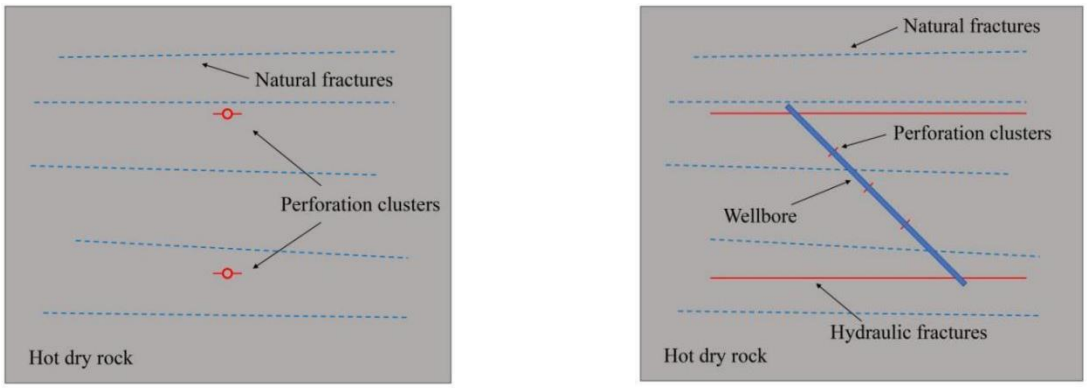

(a) **(b)**

Figure 1: Multi-stage fracturing scheme. (a) First-stage fracturing in the reverse fault formation; (b) second-stage fracturing in the reverse fault formation.

Table 1: Physical and mechanical properties of numerical models (Sun et al. 2017, Yao et al. 2018).

Parameters	Value	Unit
Rock density	2700	kg/m^3
Young's modulus	45	GPa
Poisson's ratio	0.2	1
Rock porosity	0.004	1
Rock permeability	1e-17	m^2
Maximum in-situ stress	52 - 60	MPa
Minimum in-situ stress	50	MPa
Fluid density	1000	kg/m^3
Fluid viscosity	0.001	Pa·s
Injection rate	0.001	m^3/s
First-stage fracturing time	4500	s
Second-stage fracturing time	120	s

3. RESULTS AND DISCUSSION

3.1 First-stage fracturing

This section aims to explore the variation law of in-situ stress state (direction and magnitude) in the first-stage fracturing. The two perforation clusters are placed perpendicular to the minimum in-situ stress with a distance of 100 m and injected with fracturing fluid simultaneously for 4500 s. Unlike conventional simultaneous fracturing, the perforation clusters in the first-stage fracturing are located on different wells around tunnels, which means that flow redistribution can be neglected. Additionally, drilling wells from the tunnels can notably reduce construction costs.

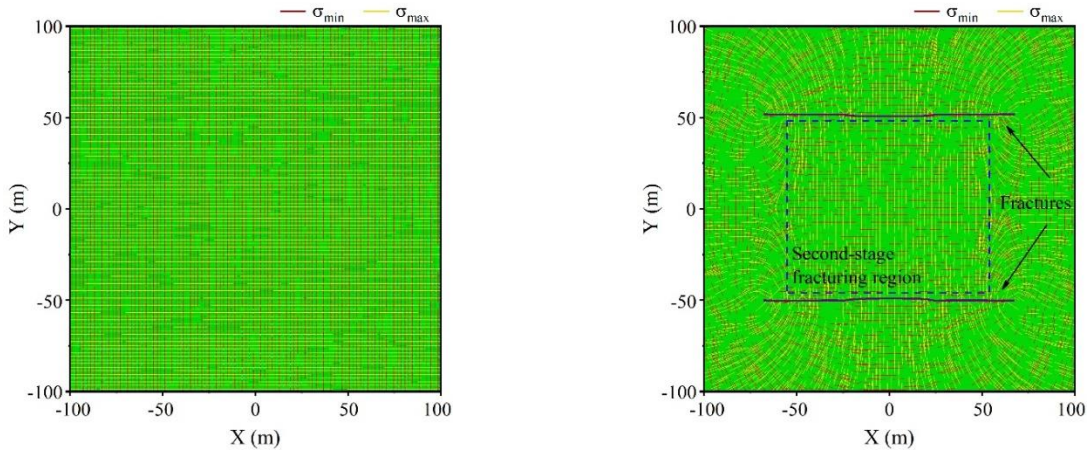

(a) **(b)**

Figure 2: In-situ stress angle. (a) Before first-stage fracturing; and (b) after first-stage fracturing.

Fig. 2 compares the in-situ stress state before and after the first-stage fracturing. Before the first-stage fracturing, the in-situ stress distribution is homogeneous, the maximum and the minimum in-situ stresses (σ_{max} and σ_{min}) are 52 MPa and 50 MPa, respectively, and the σ_{min} is vertical. Fracture propagation changes the in-situ stress balance and causes a new in-situ stress state (He et al. 2017). With the continuous injection of fracturing fluid, the fluid acts on the inner surfaces of fractures and squeezes the surrounding rock. This squeezing effect increases the stress perpendicular to fracture surfaces and rotates the in-situ stress direction. After the first-stage fracturing, the in-situ stress around fracture tips rotates slightly (Fig. 2b). The in-situ stress rotation is mainly concentrated on the sides perpendicular to fractures. In the region between fractures, the σ_{min} is rotated by nearly 90º. This region is named as the second-

stage fracturing region. Second-stage fracturing is performed in this region, and hydraulic fractures propagate along the Y-direction and intersect with the horizontal natural fractures in reverse fault formations.

Fig. 3 quantifies the in-situ stress magnitude after first-stage fracturing. Since the tensile stresses generated by fracture propagation offset the original compressive stresses in formations, the σ_{max} and σ_{min} drop by more than 25 MPa around fracture tips. But the in-situ stress difference ($\Delta\sigma$) peaks in this region, which is related to the stress concentration around fracture tips (Li et al. 2020). Figs. 3a and 3b show that the high in-situ stress region is mainly concentrated on the outside of fractures. The σ_{max} and σ_{min} in this region are about 54 MPa and 57 MPa, respectively. The σ_{min} decreases by about 2.2 MPa, and the σ_{max} increases by about 3.6 MPa in the second-stage fracturing region. In-situ stress redistribution is positively correlated with the rock displacement to a certain extent. When two fractures propagate simultaneously, the second-stage fracturing region is subjected to opposite compressive stresses, but these compressive stresses are in the same direction in the outer region of fractures, which causes the large rock displacement and high in-situ stress in the outer region of fractures. To show the in-situ stress redistribution in the second-stage fracturing region more clearly, we plotted the variation of $\Delta\sigma$ with the selected straight lines, where A-A' is the horizontal line at Y = 0 m and B-B' is the vertical line at X = 0 m (Fig. 3c). Fig. 4 shows that the $\Delta\sigma$ increases and then decreases along A-A' and B-B' in the second-stage fracturing region and reaches a peak (8.14 MPa) at the center.

The above in-situ stress redistribution law is based on a premise that the initial in-situ stress difference is 2 MPa. Whether the in-situ stress redistribution law is applicable to formations with a large initial in-situ stress difference remains to be further discussed. We keep the initial minimum in-situ stress at 50 MPa and change the initial maximum in-situ stress from 52 MPa to 60 MPa. Fig. 4 shows the variation of $\Delta\sigma$ with A-A' and B-B' under different initial in-situ stress conditions. The initial in-situ stress difference slightly affects the qualitative distribution of $\Delta\sigma$ in the second-stage fracturing region. For example, the $\Delta\sigma$ still peaks at the center, and first increases and then decreases along A-A' and B-B'. However, different initial in-situ stress differences significantly change the $\Delta\sigma$ magnitude. The $\Delta\sigma$ decreases with the increase of initial in-situ stress difference. The peak $\Delta\sigma$ decreases by 75.6% when the initial in-situ stress difference increases from 2 MPa to 10 MPa. As the initial in-situ stress difference increases further, this reduced $\Delta\sigma$ may not meet the requirements of second-stage fracturing. Therefore, in future work, the impact factors of first-stage fracturing (such as fracture spacing, fracture number, fluid injection rate and fluid viscosity) should be studied to maximize the $\Delta\sigma$ in the second-stage fracturing region.

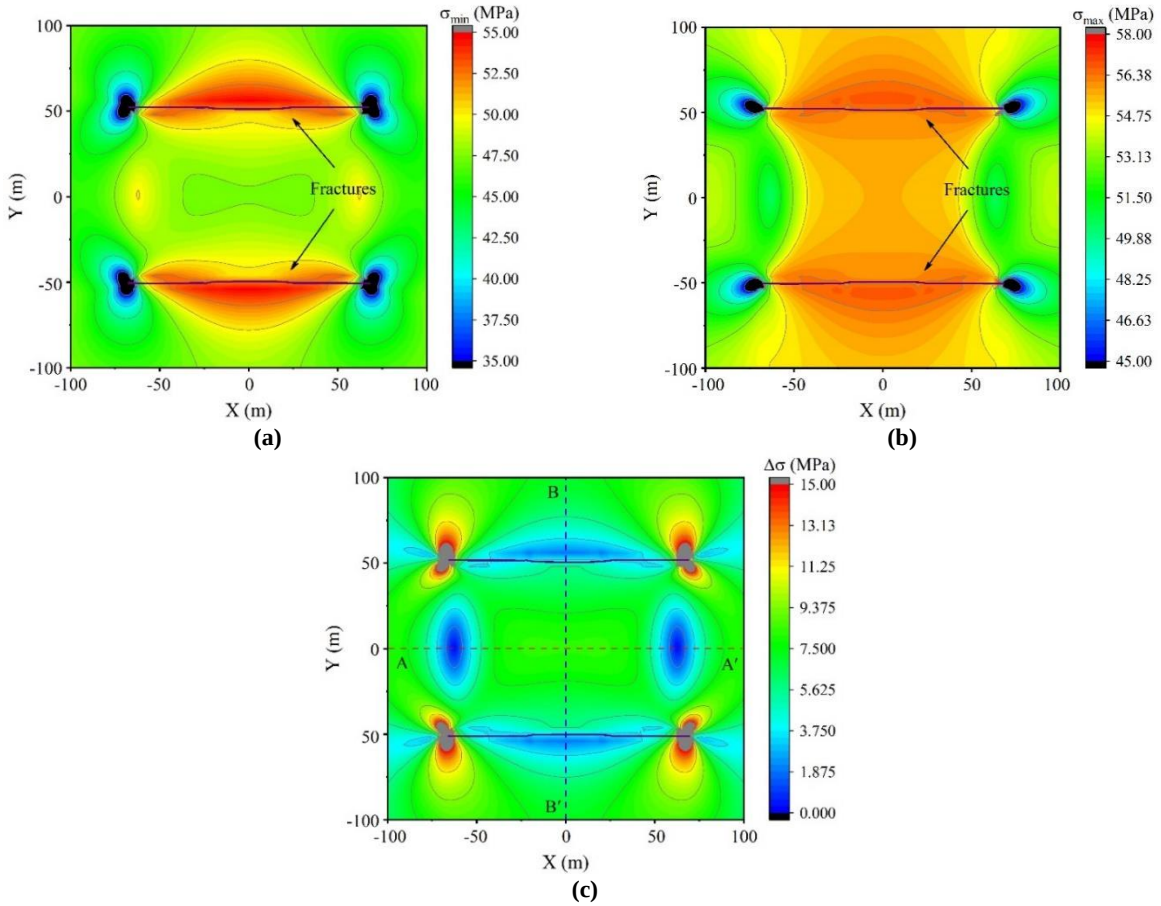

Figure 3: In-situ stress magnitude after first-stage fracturing. (a) Maximum in-situ stress; (b) minimum in-situ stress; and (c) in-situ stress difference.

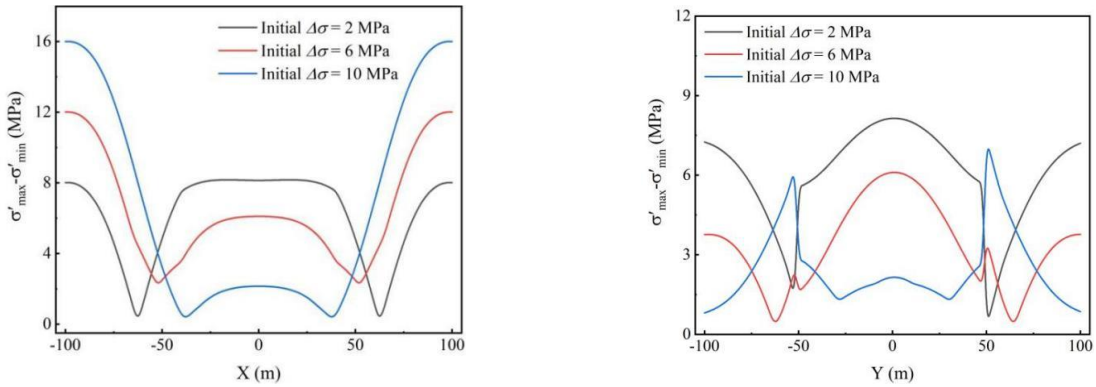

Figure 4: The variation of in-situ stress difference along A-A' and B-B'. (a) A-A'; and (b) B-B'.

3.2 Second-stage fracturing

Second-stage fracturing is used to induce desired fractures that intersect with natural fractures for improving caveability. Considering the high difficulty and cost of horizontal wells, the inclined well is drilled to perform second-stage fracturing, where the angle between the perforation clusters and the σ_{min} is 45º. Two perforation clusters are sequentially injected with fracturing fluid, and the injection time for each perforation cluster is 120 s.

Fig. 5 shows the fracture morphologies and the in-situ stress angle around fracture tips. During sequential fracturing, the first fracture (FR.1) propagates along the perforation cluster and is subsequently deflected under the influence of in-situ stress. The FR.1 propagation squeezes the surrounding rock, changes the in-situ stress state and affects the propagation of subsequent fractures, which causes the right flank of the second fracture (FR.2) to deviate significantly from the expected path (Y-direction) (Yu et al. 2020). The fracture propagation direction can be predicted by the in-situ stress angle around fracture tips. When the injection time is 92 s, the σ_{min} around the right flank tip of the FR.1 is approximately horizontal, and then the right flank of the FR.1 expands along the Y-direction. When the injection time is 232 s, around the right flank tip of the FR.2, the angle between σ_{min} and Y-direction is approximately 45º, and then the right flank of the FR.2 expands to the upper right.

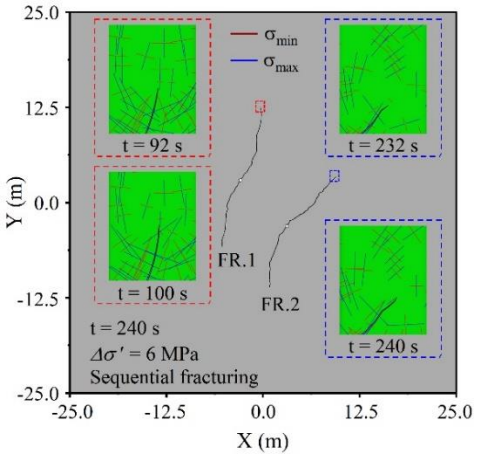

Figure 5: Fracture morphologies and the in-situ stress angle around fracture tips

Fig. 6 shows the pore pressure, fracture length and maximum fracture width in sequential fracturing. Two fractures interact with each other over sequential fracturing. The FR.1 propagation increases the pore pressure of surrounding rocks and the initiation pressure of the FR.2. The region with high pore pressure is mainly concentrated on the right side of the FR.2. In the first 120 s, the fracture length and the maximum fracture width increase with injection time. After 120 s, the FR.2 expands, generating compressive stress and squeezing the FR.1. When the injection time increases from 120 s to 240 s, the maximum fracture width of the FR.1 decreases by 12.7%, but its fracture length remains constant. This is because although the FR.2 squeezes the FR.1 and increases its internal pressure, this increased pressure is lower than the extension pressure of the FR.2 and cannot lengthen the FR.2 further. Besides, unlike the constructing flow channels in the oil/gas field, induced fractures in rock caving are used to increase rock caveability and reduce fragmentation sizes. The reduced FR.2 width has a slight effect on rock caveability. Therefore, the main focus in rock preconditioning should be on the fracture length and expansion path, ignoring the fracture width. In summary, the new stress state resulting from the first-stage fracturing favors the creation of desired hydraulic fractures that intersect with pre-existing natural fractures. But stress shadowing in multi-perforation clusters fracturing causes fractures to deviate from the expected path over the second-stage fracturing. The fracture expansion mechanism and impact factors of multi-perforation fracturing should be further investigated in future work.

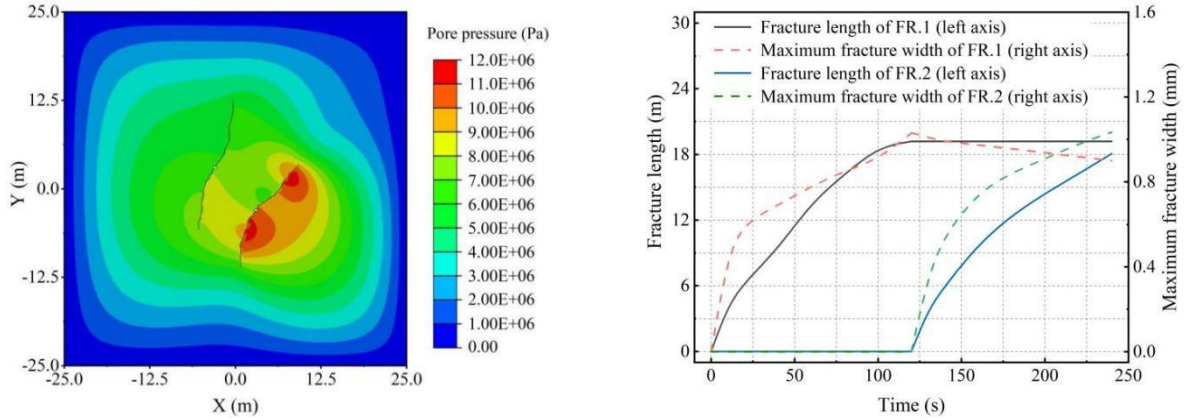

(a) **(b)**

Figure 6: Pore pressure, fracture length and maximum fracture width in sequential fracturing. (a) Pore pressure distribution; and (b) variation of fracture length and maximum fracture with injection time.

4. CONCLUSION

In this study, we proposed a multi-stage fracturing method to control the fracture trajectory for enhancing rock caveability. The first-stage fracturing is used to optimize the in-situ stress state based on stress shadowing. Then, the desired fractures intersecting with natural fractures are induced in the second-stage fracturing to unravel the whole rock into blocks.

We found that the fracture propagation changes the original in-situ stress balance and causes a new in-situ stress state. After the first-stage fracturing, the in-situ stress angle changes slightly, but the new in-situ stress difference peaks around fracture tips. In the second-stage fracturing region, the minimum in-situ stress is rotated by nearly 90º and the new in-situ stress difference is about 8 MPa. The new in-situ stress difference decreases with the increase of initial in-situ stress difference in this region. Choosing appropriate construction parameters is necessary to optimize the new in-situ stress difference. Multiple fractures interact with each other over second-stage fracturing; the first fracture propagation increases the pore pressure of surrounding rocks and alters the trajectory of the second fracture; and the second fracture squeezes the first fracture and reduces its width.

This study provides a new method for rock preconditioning and benefits the reservoir construction of excavation-based enhanced geothermal system. However, rock inhomogeneities (e.g., natural fractures and property anisotropy) were neglected in this study and should be further discussed in future work.

REFERENCE

Haraden, J.: The status of hot dry rock as an energy source, *Energy*, **17**, (1992), 777-786.

He, Q., Suorineni, F., Ma, T., and Oh, J.: Effect of discontinuity stress shadows on hydraulic fracture re-orientation, *International Journal of Rock Mechanics and Mining Sciences*, **91**, (2017), 179-194.

He, Q., Suorineni, F., and Oh, J.: Review of hydraulic fracturing for preconditioning in cave mining, *Rock Mechanics and Rock Engineering*, **49**, (2016), 4893-4910.

Joubert, P.: Microseismic monitoring of hydraulic fractures in block cave mines, *Mining Technology*, **119**, (2010), 193-197.

Kang, F., and Tang, C.: Overview of enhanced geothermal system (EGS) based on excavation in China, *Earth Science Frontiers*, **27**, (2020), 185-193.

Li, S., Wang, S., and Tang, H.: Stimulation mechanism and design of enhanced geothermal systems: A comprehensive review, *Renewable and Sustainable Energy Reviews*, **155**, (2022), 111914.

Li, Y., Long, M., Tang, J., Chen, M., and Fu, X.: A hydraulic fracture height mathematical model considering the influence of plastic region at fracture tip, *Petroleum Exploration and Development*, **47**, (2020), 184-195.

Li, Y., Sun, W., Kang, F., and Tang, C.: Heat extraction efficiency in deep geothermal energy mining and implications for EGS-E, *Chinese Journal of Engineering*, **44**, (2022), 1-10.

Liu, Y., Li, W., Wang, X., and Xia, C.: Pre-conditioning technology by hydraulic fracturing and its application practice in a block caving mine, *China mine engineering*, **51**, (2022), 26-32.

Rafiee, R., Ataei, M., Khalokakaie, R., Jalali, S., and Sereshki, F.: Determination and assessment of parameters influencing rock mass cavability in block caving mines using the probabilistic rock engineering system, *Rock Mechanics and Rock Engineering*, **48**, (2015), 1207-1220.

Rafiee, R., Ataei, M., Khalokakaie, R., Jalali, S., and Sereshki, F.: A fuzzy rock engineering system to assess rock mass cavability in block caving mines, *Neural Computing and Applications*, **27**, (2016), 2083-2094.

Sun, Z., Zhang, X., Xu, Y., Yao, J., Wang, H., Lv, S., Sun, Z.-L., Huang, Y., Cai, M., and Huang, X.: Numerical simulation of the heat extraction in EGS with thermal-hydraulic-mechanical coupling method based on discrete fractures model, *Energy*, **120**, (2017), 20-33.

Wang, G., Lin, W., Zhang, W., Lu, C., Ma, F., and Gan, H.: Research on formation mechanisms of hot dry rock resources in China, *Acta Geologica Sinica-English Edition*, **90**, (2016), 1418-1433.

Wang, Z., Tang, Y., and Gong, H.: Longwall Top-Coal Caving Mechanism and Cavability Optimization with Hydraulic Fracturing in Thick Coal Seam: A Case Study, *Energies*, **14**, (2021), 1-17.

Yao, J., Zhang, X., Sun, Z., Huang, Z., Liu, J., Li, Y., Xin, Y., Yan, X., and Liu, W.: Numerical simulation of the heat extraction in 3D-EGS with thermal-hydraulic-mechanical coupling method based on discrete fractures model, *Geothermics*, **74**, (2018), 19-34.

Yu, L., Wu, X., Hassan, N., Wang, Y., Ma, W., and Liu, G.: Modified zipper fracturing in enhanced geothermal system reservoir and heat extraction optimization via orthogonal design, *Renewable Energy*, **161**, (2020), 373-385.

Zhao, J., Tang, C., and Wang, S.: Excavation based enhanced geothermal system (EGS-E): introduction to a new concept, *Geomechanics and Geophysics for Geo-Energy and Geo-Resources*, **6**, (2020), 1-7.